ELSEVIER

Applied Mathematical Modelling 26 (2002) 545–561

APPLIED MATHEMATICAL MODELLING

www.elsevier.com/locate/apm

An analytical solution for conduction-dominated unidirectional solidification of binary mixtures

Suman Chakraborty [1], Pradip Dutta *

Department of Mechanical Engineering, Indian Institute of Science, Bangalore 560 012, India

Received 4 September 2000; received in revised form 30 April 2001; accepted 3 July 2001

Abstract

In this paper, a fully analytical solution technique is established for the solution of unidirectional, conduction-dominated, alloy solidification problems. By devising appropriate averaging techniques for temperature and phase-fraction gradients, governing equations inside the mushy region are made inherently homogeneous. The above formulation enables one to obtain complete analytical solutions for solid, liquid and mushy regions, without resorting to any numerical iterative procedure. Due considerations are given to account for variable properties and different microscopic models of alloy solidification (namely, equilibrium and non-equilibrium models) in the two-phase domain. The results are tested for the problem of solidification of a NH_4Cl–H_2O solution, and compared with those from existing analytical models as well as with the corresponding results from a fully numerical simulation. The effects of different microscopic models on solidification behaviour are illustrated, and transients in temperature and heat flux distribution are also analysed. A good agreement between the present solutions and results from computational simulation is observed.

Keywords: Fully analytical; Conduction dominated; Unidirectional solidification; Binary alloy; Mushy region

1. Introduction

Unidirectional solidification can occur in a rectangular cavity if it is cooled from the bottom. Such a system is thermally stable if the Rayleigh number is low, and hence conduction can be the dominating mode of heat transport. This situation is not only relevant in nature and in practical applications such as materials processing and crystal growth, but also provides us with an

* Corresponding author. Tel.: +91-3-3444111x2332; fax: +91-8-3600648.
E-mail address: pradip@mecheng.iisc.ernet.in (P. Dutta).
[1] On leave from Department of Power Plant Engineering, Jadavpur University, Calcutta 700 091, India.

0307-904X/02/$ - see front matter
PII: S0307-904X(01)00073-7

Nomenclature

a	a constant based on ratio of thermophysical properties
b	a constant based on ratio of thermophysical properties
C	species concentration
c	specific heat
F	function
g	volume fraction of concerned phase
k	thermal conductivity
k_P	partition coefficient
L	latent heat of fusion
q	heat flux
r	ratio of certain thermophysical properties (constant)
St	Stefan number
T	temperature
t	time
x	coordinate variable

Greek symbols

α	thermal diffusivity
η	similarity variable
ρ	density
θ	dimensionless temperature

Subscripts

C	cold surface
E	eutectic
eq	equivalent
i	initial
L	liquid phase
liq	liquidus
M	mushy
melt	at melting point
S	solid phase
sol	solidus

opportunity for analytical treatment. Analytical solutions are important for accurate investigation of solidification behaviour of a wide variety of materials, since experimental or numerical techniques are often difficult and expensive in this field. Further, analytical solutions can give us a deeper physical insight into the problem under investigation.

The family of closed-form solutions to melting–solidification problems is mainly associated with the processes addressing the phase change of pure substances. In those materials, the phase change takes place isothermally. However, most actual solidification processes involve alloys rather than pure materials. The complexity of such problems with regard to temperature distri-

bution and the solidification rate is much greater than those involving pure materials. This is primarily because of the phase change process occurring over a range of temperature and involving a two-phase or mushy zone, where both liquid and solid phases coexist.

It is generally observed in the literature that most analytical solution techniques pertaining to the solid and liquid regions are somewhat straightforward. However, in the mushy region, the solutions are usually obtained after assuming different degrees of simplification. In the literature, only a few fully analytical treatment of the mushy zone have been reported. For example, Tien and Geiger [1] analysed the directional solidification of a system by assuming the solid fraction to be linearly varying with distance within the freezing zone between the solidus and the liquidus fronts. It was also assumed that the physical properties are independent of temperature and solid fraction. An approximate method, namely the heat balance integral method, was employed for solving the governing equations. Cho and Sunderland [2] presented an exact solution for the temperature distribution and rate of phase change for a semi-infinite body where the phase change occurred over a range of temperature. This solution assumed constant thermophysical properties and a linear variation of solid fraction with distance from the liquidus front. Muehlbauer et al. [3] performed an analysis of transient one-dimensional solidification of a superheated finite slab of binary alloy. In this case, too, all physical properties were assumed to remain constant and the governing equations were solved using a heat balance integral method. Ozisik and Uzzel [4] obtained an exact solution for freezing in a cylindrically symmetric system with an extended freezing temperature range. A constant property assumption was made, and the solid fraction was assumed to vary linearly with length as well as temperature. Worster [5], however, assumed variable property in the solution of a conduction-dominated directional alloy solidification problem. Worster [5] formulated a mathematical model for the region of dendritic or cellular growth, for the case of unidirectional solidification of an alloy from a plane wall. It was assumed that transport of heat and solute is by diffusion alone, and the model was closed by a condition of marginal equilibrium. However, regarding solution of the system of governing differential equations for the mushy region, a numerical solution technique, namely the "shooting method", was employed. It can be noted that the analytical solution methods followed in the above studies are essentially similarity transformation techniques [6,7] adopted to solve transient, unidirectional, heat conduction problems. Such transformation, in fact, are quite similar to the Landau transformation presented in [8]. Subsequently, numerical solutions have also been attempted in the literature to solve similar problems, using iterative procedures for obtaining interface locations [9] or well-known finite-difference methods [10] to obtain the temperature field. However, to the best of our knowledge, no study has yet been reported that attempted to obtain the temperature profile in the mushy zone in a closed form, with proper incorporation of metallurgically consistent phase change considerations.

In the present work, a fully analytical technique for the solution of transient, conduction-dominated, directional solidification problems of binary alloys is outlined. This is achieved by using a purely analytical technique to incorporate the phase-diagram information, composition–solid fraction coupling and variation of physical properties inside the mushy region. The objective of the present formulation is to correlate the variation of solid-fraction assumption with the information obtained from a corresponding metallurgical phase diagram, and hence appropriately represent the coupling between the temperature and solid fraction in the two-phase region, without adhering to any kind of numerical technique. In order to do so, a weighted averaging

technique for the determination of temperature and phase-fraction gradients inside the mushy region is devised, that homogenises the system of governing equations. The results are tested for the problem of solidification of a NH_4Cl–H_2O solution, and then compared with the corresponding results from a numerical simulation.

2. Mathematical formulation and analysis

2.1. The governing equations

A schematic diagram of the physical model is depicted in Fig. 1, in which a binary mixture is cooled to solidify in a direction perpendicular to an isothermal cold wall. The following are the assumptions made in the analysis of the above solidification problem:

1. The physical properties within both the solid part and the freezing zone are independent of temperature, but may be different in each zone.
2. The volume change during the entire solidification process is negligible. Moreover, liquid and solid densities are assumed to be equal and constant. Hence, the volume fraction and mass fraction of any phase are identical.
3. The temperature varies only along the x-direction.
4. Conduction is the only heat transfer mechanism within the system.
5. The temperature–composition coupling is according to a metallurgical phase diagram.

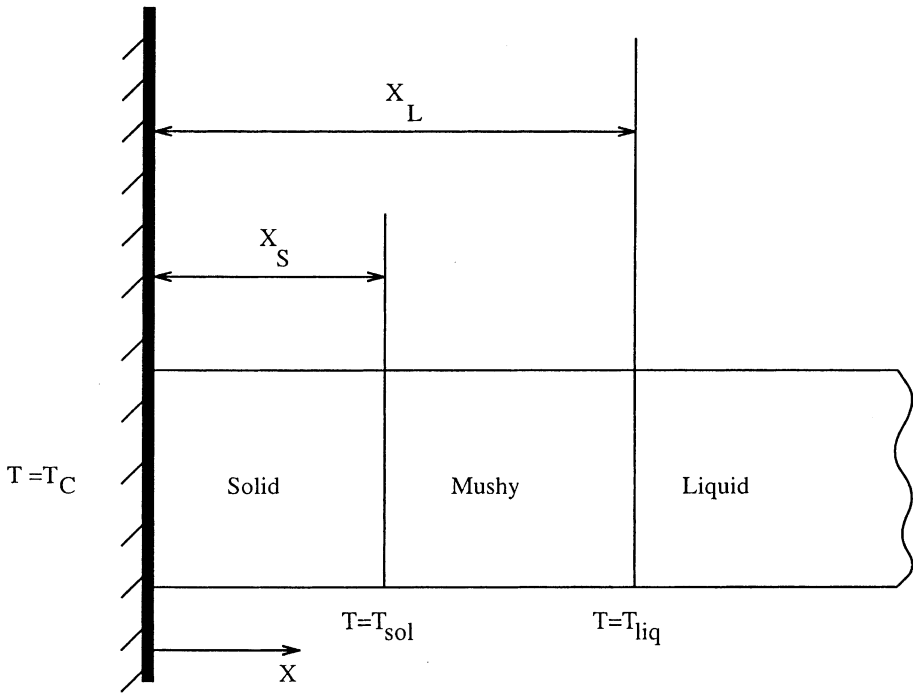

Fig. 1. A schematic diagram of the physical problem.

6. The coupling between species composition and phase fraction can be according to an equilibrium rule (lever rule) or a non-equilibrium rule (Scheil's equation), as outlined in [11].
7. Except for density, the other physical properties in the mushy region are interpolated as linear functions of the average mass fraction of the solid.
8. Macroscopic species diffusion is negligible compared to thermal diffusion.

Using the above assumptions, the model equations describing the temperature distributions in each region can be written as

$$\frac{1}{\alpha_S}\frac{\partial T_S}{\partial t} = \frac{\partial^2 T_S}{\partial x^2} \quad \text{for } 0 < x < x_S, \tag{1}$$

$$\frac{1}{\alpha_M}\frac{\partial T_M}{\partial t} = \frac{\partial^2 T_M}{\partial x^2} + \frac{\rho L}{k_M}\frac{\partial g_S}{\partial t} \quad \text{for } x_S < x < x_L, \tag{2}$$

$$\frac{1}{\alpha_L}\frac{\partial T_L}{\partial t} = \frac{\partial^2 T_L}{\partial x^2} \quad \text{for } x_L < x < \infty. \tag{3}$$

In Eqs. (1)–(3), the subscripts S, L, and M refer to the solid, liquid and the mushy zones, respectively, and g refers to the volume fraction. The second term on the right-hand side of Eq. (2) accounts for the heat generated in the mushy region by the creation of the solid dendrites or other crystalline structures constituting the solid matrix in the mushy zone. Using the chain rule,

$$\frac{\partial g_S}{\partial t} = \frac{\partial g_S}{\partial T_M}\frac{\partial T_M}{\partial t}. \tag{4}$$

Using Eq. (4), Eq. (2) can be written as:

$$\left(\frac{1}{\alpha_M} - \frac{\rho L}{k_M}\frac{\partial g_S}{\partial T_M}\right)\frac{\partial T_M}{\partial t} = \frac{\partial^2 T_M}{\partial x^2} \quad \text{for } x_S < x < x_L. \tag{5}$$

2.2. Interface and boundary conditions

The matching conditions at the interfaces and the boundary conditions for the solution of governing equations (1), (3) and (5) are as follows (refer to Fig. 1):

$$\text{At } x = 0, \quad T_S = T_C, \tag{6}$$

$$\text{At } x = x_S, \quad T_S = T_M = T_{sol}, \tag{7}$$

$$k_S\left(\frac{\partial T_S}{\partial x}\right)_{x=x_S} - k_M\left(\frac{\partial T_M}{\partial x}\right)_{x=x_S} = \rho L_{eq}(1 - g_{S,sol})\frac{dx_S}{dt}, \quad \text{where } L_{eq} = (c_L - c_S)T_{sol} + L, \tag{8}$$

$$\text{At } x = x_L, \quad T_M = T_L = T_{liq}, \tag{9}$$

$$k_M\left(\frac{\partial T_M}{\partial x}\right)_{x=x_L} - k_L\left(\frac{\partial T_L}{\partial x}\right)_{x=x_L} = \rho L_{eq} g_{S,liq}\frac{dx_L}{dt}, \tag{10}$$

$$\text{At } x \to \infty, \quad T_L = T_i. \tag{11}$$

2.3. Non-dimensionalisation

Using the following non-dimensional parameters:

$$\theta_S = \frac{T_S - T_C}{T_{sol} - T_C}, \quad \theta_M = \frac{T_M - T_{sol}}{T_{melt} - T_{sol}}, \quad \theta_L = \frac{T_L - T_i}{T_{liq} - T_i},$$

Eqs. (1), (3) and (5) can be non-dimensionalised as:

$$\frac{1}{\alpha_S}\frac{\partial \theta_S}{\partial t} = \frac{\partial^2 \theta_S}{\partial x^2}, \tag{12}$$

$$\frac{1}{\alpha_{M'}}\frac{\partial \theta_M}{\partial t} = \frac{\partial^2 \theta_M}{\partial x^2}, \tag{13}$$

where

$$\frac{1}{\alpha_{M'}} = \frac{1}{\alpha_M} - \frac{\rho L}{k_M}\frac{\partial g_S}{\partial T_M}, \tag{14}$$

$$\frac{1}{\alpha_L}\frac{\partial \theta_L}{\partial t} = \frac{\partial^2 \theta_L}{\partial x^2}. \tag{15}$$

2.4. Similarity transformation

A similarity transformation of the form $\eta = xg(t)$, where $g(t) = 1/2\sqrt{\alpha_S t}$ is applied, which converts the system of partial differential equations (12)–(15) into a set of ordinary differential equations as follows:

$$\frac{d^2 \theta_S}{d\eta^2} + 2\eta\frac{d\theta_S}{d\eta} = 0 \quad \text{for } 0 < \eta < \eta_S, \tag{16}$$

$$\frac{d^2 \theta_M}{d\eta^2} + 2\frac{\alpha_S}{\alpha_{M'}}\eta\frac{d\theta_M}{d\eta} = 0 \quad \text{for } \eta_S < \eta < \eta_L, \tag{17}$$

where

$$\frac{\alpha_S}{\alpha_{M'}} = \frac{c_M - L(\partial g_S/\partial T_M)}{c_S(k_M/k_S)}, \tag{18}$$

$$\frac{d^2 \theta_L}{d\eta^2} + \frac{2k_S c_L}{k_L c_S}\eta\frac{d\theta_L}{d\eta} = 0 \quad \text{for } \eta_L < \eta < \infty. \tag{19}$$

The sequential steps for deriving Eqs. (16)–(19) from the governing partial differential equations (12)–(15), using similarity solution techniques, are detailed in Appendix A.

The boundary conditions consistent with Eqs. (16)–(19) are as follows:

$$\text{At } \eta = 0, \quad \theta_S = 0, \tag{20}$$

$$\text{At } \eta = \eta_S, \quad \theta_S = 1, \tag{21}$$

$$\theta_M = 0, \tag{22}$$

$$\theta_E \frac{d\theta_S}{d\eta} - r_{MS} \frac{d\theta_M}{d\eta} = \frac{2\eta(1 - g_{S,sol})}{St}, \tag{23}$$

where

$$\theta_E = \frac{T_{sol} - T_C}{T_{melt} - T_{sol}}, \tag{24}$$

$$r_{MS} = \frac{k_M}{k_S}, \tag{25}$$

$$St = \frac{c_S(T_{melt} - T_{sol})}{L_{eq}}. \tag{26}$$

$$\text{At } \eta = \eta_L, \quad \theta_M = \theta_{liq} = \frac{T_{liq} - T_{sol}}{T_{melt} - T_{sol}}, \tag{27}$$

$$\theta_L = 1, \tag{28}$$

$$r_{MS} \frac{d\theta_M}{d\eta} - r_{LS}\theta_i \frac{d\theta_L}{d\eta} = \frac{2g_{S,liq}\eta}{St}, \tag{29}$$

where

$$r_{LS} = \frac{k_L}{k_S}, \tag{30}$$

and

$$\theta_i = \frac{T_{liq} - T_S}{T_{melt} - T_{sol}}. \tag{31}$$

$$\text{At } \eta \to \infty, \quad \theta_L = 0. \tag{32}$$

2.5. Solution of the governing equations

The solution for the solid and liquid regions can be obtained in a straightforward manner, and the results are as follows:

$$T_S = T_C + (T_{sol} - T_C)\frac{\operatorname{erf}(\eta)}{\operatorname{erf}(\eta_S)} \quad \text{for } 0 < \eta < \eta_S, \tag{33}$$

$$T_L = T_i + (T_{liq} - T_i)\frac{\operatorname{erfc}(\sqrt{b}\eta)}{\operatorname{erfc}(\sqrt{b}\eta_L)} \quad \text{for } \eta_L < \eta < \infty, \tag{34}$$

where $b = k_S c_L / k_L c_S$ and erfc = 1 − erf.

However, solution for the mushy region is not straightforward and requires further analysis. In the known analytical studies found in the literature [1–4], a linear variation of solid fraction with temperature (or length) is prescribed and/or a constant property assumption is imposed, in order to obtain a closed-form expression for the temperature profile in the mushy region. However, such assumptions may oversimplify the problem, and may yield inconsistent results, since the information regarding the phase diagram and that of the composition–solid fraction coupling are not incorporated. The main objective here is to represent the variation of solid fraction with temperature inside the mushy region as consistently as possible with the metallurgy. The added objective here is to avoid any kind of numerical approximation for this matter, in order to retain the analytical nature of the final solution. For that purpose, a general guideline is proposed, as described below. For the purpose of illustration, a linearised phase diagram is considered (refer to Fig. 2), for which the following equation can be written:

$$\frac{T_M - T_{melt}}{T_{sol} - T_{melt}} = \frac{C_S}{C_i}. \tag{35}$$

The next step is to incorporate the composition vs. melt-fraction coupling, which may be governed by equilibrium solidification, based on lever rule [11], as

$$\frac{C_S}{C_i} = \frac{1}{g_S + (1 - g_S)/k_P} \tag{36}$$

or, by non-equilibrium solidification, based on Scheil's equation [11], as

$$\frac{C_L}{C_i} = (1 - g_S)^{(k_P - 1)}. \tag{37}$$

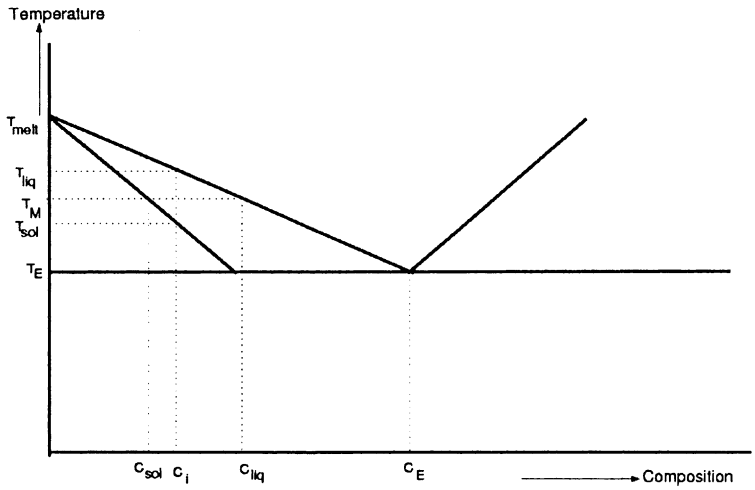

Fig. 2. A typical linearised phase diagram.

Combining Eqs. (35)–(37), the relationship between solid fraction and temperature can be expressed as:

For equilibrium solidification:

$$\frac{\partial g_S}{\partial T_M} = \frac{1}{1 - 1/k_P} \frac{(T_{melt} - T_{solid})}{(T_M - T_{melt})^2}. \tag{38}$$

For non-equilibrium solidification:

$$\frac{\partial g_S}{\partial T_M} = \frac{1}{(1 - k_P)k_P} \left(\frac{1}{T_{solid} - T_{melt}} \right)^{[1/(k_P - 1)]} \cdot (T_M - T_{melt})^{[(2-k_P)/(k_P-1)]}. \tag{39}$$

Now, Eq. (17) can be analytically solved to yield a metallurgically consistent solution, only when a proper estimation of a representative value of $\partial g_S/\partial T_M$ is made in expression (18). It is apparent from Eqs. (38) and (39) that the partial differentials appearing in these equations vary with temperature throughout the solidification domain. Hence, prescription of a representative value of $(\partial g_S/\partial T_M)$ (represented as g'_S) can be made by defining it as follows:

$$g'_S = \left(\int_{T_{sol}}^{T_{liq}} \frac{\partial g_S}{\partial T_M} \mathrm{d}T_M \Big/ \Delta T \right), \quad \text{where } \Delta T = T_{liq} - T_{sol}. \tag{40}$$

At this stage, it is important to explain the significance of such averaging of solid-fraction gradients across the solidification interval. The main purpose of doing so is to conceptually obtain an equivalent temperature of phase change, which is metallurgically consistent with the model adopted (for instance, lever rule or Scheil's model), so that an equivalent solid fraction can be calculated, based on the respective rule. This leads to a situation in which analytical solution for the mushy region can be achieved. It may be realised that no analytical solution can be obtained if one uses an exact representation of variation of solid-fraction gradients within the mushy region. As a practical alternative, we aim for a closed-form solution algorithm that inherently contains metallurgical information of the concerned model, as consistently as possible. Even with this simplified definition of equivalent solid fraction, one does not lose the information conveyed by the corresponding model. This issue has not been specifically addressed in earlier literature pertaining to closed-form solution of similar problems.

Eq. (40) can be applied to either of Eqs. (38) or (39). For the purpose of illustration, the case of equilibrium solidification (based on the lever rule) is considered, for which case g'_S turns out to be:

$$g'_S = \frac{1}{(1 - 1/k_P)(T_{melt} - T_{liq})}. \tag{41}$$

Eq. (41) is exactly true for a representative temperature (T_{eq}) in the mushy region, which can be obtained by simultaneously using Eqs. (38) and (41) as

$$T_{eq} = T_{melt} - \sqrt{T_{melt}^2 - T_{melt}T_{liq} - T_{melt}T_{sol} + T_{sol}T_{liq}}. \tag{42}$$

The representative value of g_S, i.e., $g_{S,eq}$, can now be calculated by combining Eqs. (35) and (36) as

$$g_{S,eq} = \frac{1}{1 - 1/k_P} \left(\frac{T_{melt} - T_{sol}}{T_{melt} - T_{eq}} - \frac{1}{k_P} \right). \tag{43}$$

Now, all the properties in the mushy region can effectively be represented by interpolating on the basis of the expressions above. Thus, the whole procedure for consistent representation of expression (18) can be summarised as follows:

Step 1: Express the phase diagram in a form $T_M = F_1(C_L)$, where F_1 represents a mathematical function.

Step 2: Express C_L as: $C_L = F_2(g_S)$, using the governing rule of solidification (where F_2 represents a mathematical function).

Step 3: Combine steps 1 and 2 to obtain $T_M = F_1F_2(g_S) = F_3(g_S)$, say, where F_3 is a mathematical function. The governing rule of solidification, for example, can be lever rule (Eq. (36)) or Scheil's equation (Eq. (37)).

Step 4: Calculate $\partial g_S/\partial T_M$ from step 3.

Step 5: Using Eq. (40) and step 4, obtain a representative value g'_S.

Step 6: Obtain representative values of T and g_S (namely T_{eq} and $g_{S,eq}$, respectively) using step 5.

Step 7: Interpolate physical properties by using results from step 6.

A systematic execution of above steps leads to the solution within the mushy region as

$$T_M = T_{sol} + \left(T_{liq} - T_{sol}\right)\frac{\operatorname{erf}(\sqrt{a}\eta) - \operatorname{erf}(\sqrt{a}\eta_L)}{\operatorname{erf}(\sqrt{a}\eta_L) - \operatorname{erf}(\sqrt{a}\eta_S)}, \quad \text{where } a = \frac{\alpha_S}{\alpha'_M}, \ \eta_S < \eta < \eta_L. \tag{44}$$

Now, using Eqs. (33), (34) and (44), temperature variation within the solid, liquid and the mushy region, respectively, can be obtained, provided values for η_S and η_L can be estimated. For that purpose, the interface boundary conditions (23) and (29) can be utilised. Combining those conditions with Eqs. (33), (34) and (44), one obtains:

$$\frac{\theta_E \exp(-\eta_S^2)}{\operatorname{erf}(\eta_S)} - \frac{\sqrt{a} r_{MS}\theta_{liq}\exp(-a\eta_S^2)}{\operatorname{erf}(\sqrt{a}\eta_L) - \operatorname{erf}(\sqrt{a}\eta_S)} = \frac{\sqrt{\pi}\eta_S(1 - g_{S,sol})}{St}, \tag{45}$$

$$\frac{\sqrt{a}\theta_{liq} r_{MS}\exp(-a\eta_L^2)}{\operatorname{erf}(\sqrt{a}\eta_L) - \operatorname{erf}(\sqrt{a}\eta_S)} + \frac{\sqrt{b} r_{LS}\theta_i \exp(-b\eta_L^2)}{\operatorname{erfc}(\sqrt{b}\eta_L)} = \frac{\sqrt{\pi}\eta_L g_{S,liq}}{St}. \tag{46}$$

Eqs. (45) and (46) can now be simultaneously solved to obtain values of η_S and η_L.

3. Results and discussion

For the assessment of the present solution, results are obtained from a numerical simulation of the continuum energy conservation equation. The governing equation can be arrived at by switching off the advective terms in the general energy conservation equation [12]. For numerical solution of the above equation, the problem domain is discretised using a fixed grid enthalpy based finite volume procedure [13]. Since the sole purpose of referring to the numerical solution is to compare with the results from the full analytical solution, the computational method is not described here in details for the sake of brevity. Details of the computational method can be found in the literature [14]. The working medium for the model situation is chosen to be a NH_4Cl–H_2O solution, with 70% initial concentration (mass fraction of water), the physical properties for which are tabulated in [13]. It can be noted that our numerical code was first validated against typical

solidification problems quoted in the literature [13], before using it for the solution of the present problem.

Fig. 3 shows a comparison of the temperature distribution inside the problem domain between the present results and those from other fully analytical studies reported in the literature with different modelling assumptions [1–5]. The figure also includes a comparison between the present analytical solution and the results from an established numerical model [12], and the agreement is found to be excellent. From the same figure, it can also be observed that assumptions of constant properties for the solid and the liquid can result in a significant deviation from the present solution. In addition, the results are seen to deviate if one makes the assumption of linear variation of solid fraction with length or temperature. Such a deviation is likely to be amplified if the initial concentration (C_i) of the alloy is significantly different from the eutectic point concentration, resulting in a considerable difference between T_{liq} and T_{sol}. With a linear variation of temperature (or solid fraction) from liquidus to solidus, the transition from liquid state to solid state takes place over a shorter distance, resulting in a thinner mushy region. In Fig. 3, the present analytical and numerical results are produced using Scheil's model [11] to model microscopic species distribution.

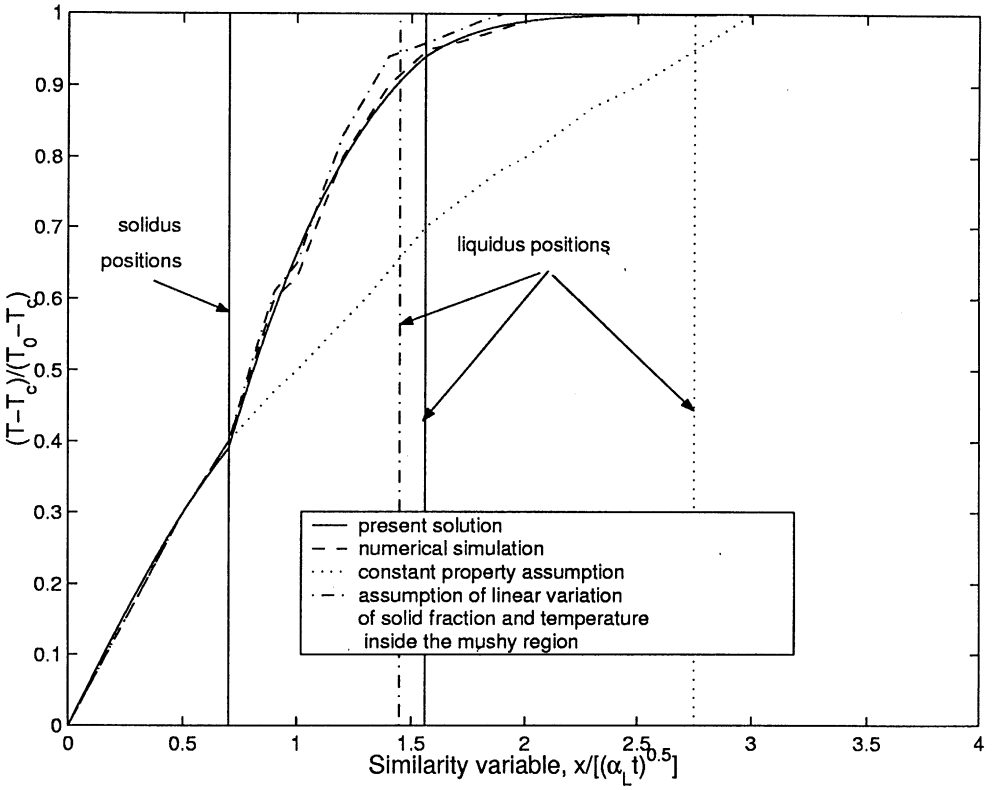

Fig. 3. Non-dimensional temperature distribution for various models. The vertical line showing the solidus positions is common for all the models. The vertical lines showing the liquidus positions correspond to various models as shown in the legend. The liquidus positions for the present solution and for the numerical solution coincide.

The effect of microscopic species transport model is shown in Fig. 4, which shows the variation of solid fraction with distance for the two microscopic models, namely the lever rule and Scheil's model, as defined in Eqs. (36) and (37), respectively. Here, it is observed that the two microscopic models do not yield identical results. Although there is no appreciable difference in interface locations for the two cases, there is a noticeable difference in variation of solid fraction. With the model based on Scheil's equation, the solid fraction seems to be less than that corresponding to the one based on lever rule, especially near the solidus. This difference can be attributed to the assumption of infinitely large solute diffusion coefficient in the solid state (microscopic) in the lever rule model, as compared to a negligible value of the same assumed in the Scheil's model. Such variations could not be captured by the known previous analytical studies addressing the same problem.

The growth of the solidified front and the liquid front is shown in Fig. 5. Since $\eta_L > \eta_S$ and $\alpha_S > \alpha_L$, the liquidus front is observed to grow faster than the solidus front. The temperature distribution within the solidified portion is plotted in Fig. 6. Fig. 7 represents a plot showing the rate of heat extraction from the system, which is evaluated as

$$|q_{x=0}| = \frac{k_S(T_{sol} - T_C)}{(\sqrt{\pi\alpha_S t})\mathrm{erf}(\eta_S)}. \tag{47}$$

It is observed from Fig. 7 that as time progresses, the heat flux decreases asymptotically, indicating a decaying effect of the initial transients. In fact, a considerably smaller rate of cooling is subse-

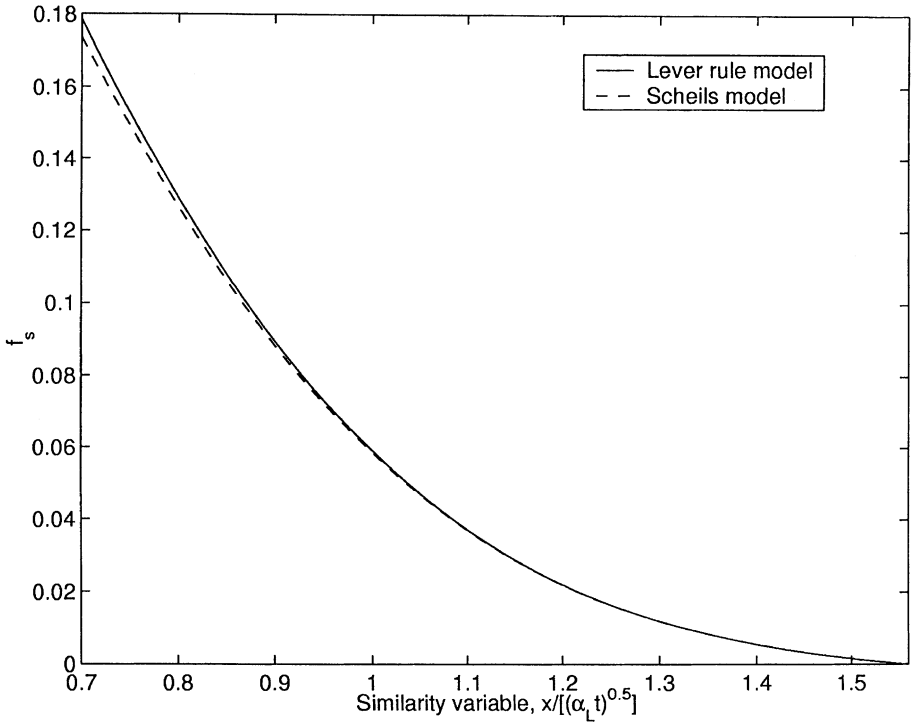

Fig. 4. Comparison of the two microscopic models with respect to solid-fraction distribution.

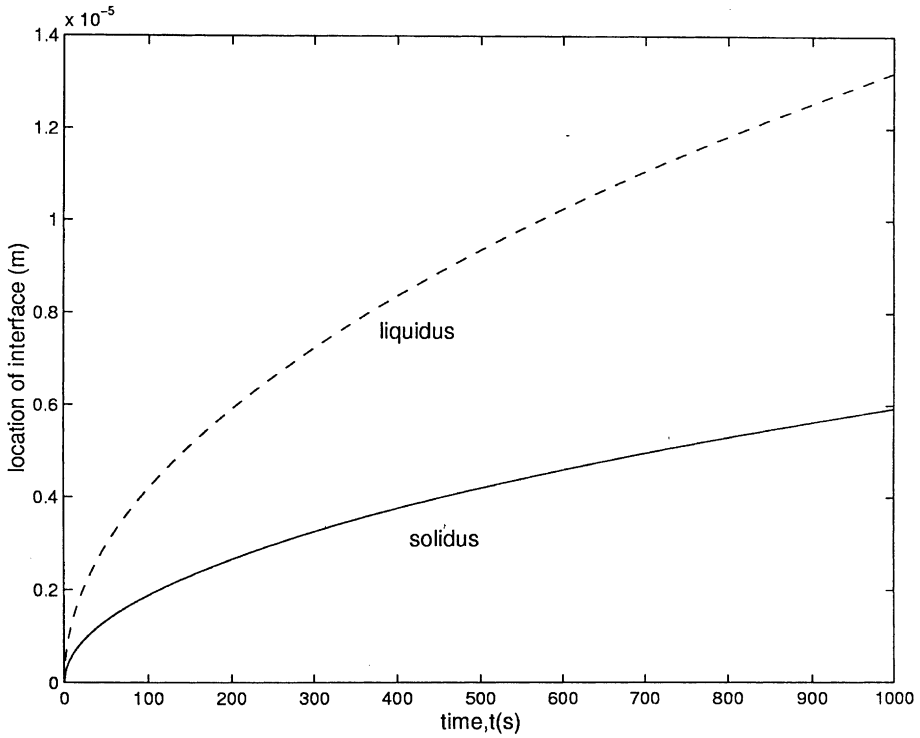

Fig. 5. Variation of location of liquidus and solidus interfaces with time.

quently needed to sustain a continuous growth of the solidification front, compared to that required to initiate the onset of solidification by creating stable nucleation sites.

4. Conclusions

In the present study, a fully analytical technique is established for the solution of transient, one-dimensional, conduction-dominated alloy solidification problems. Suitable averaging techniques for the calculation of temperature and phase-fraction gradients are devised to obtain completely analytical solutions, not only for the solid and liquid zones, but also for the mushy zone, without resorting to any sort of numerical technique. The results so obtained are compared with those from a benchmark numerical model, and an excellent agreement is observed. Insights are developed on the effect of different microscopic models on the solidification process. Variations of temperature and boundary heat flux are also analysed.

Appendix A. Derivation of similarity transformations leading to Eqs. (16)–(19) [15]

Using the similarity transformation $\eta = xg(t)$, we have:

$$\frac{\partial \theta_S}{\partial t} = x\frac{dg}{dt}\frac{d\theta_S}{d\eta}, \tag{A.1}$$

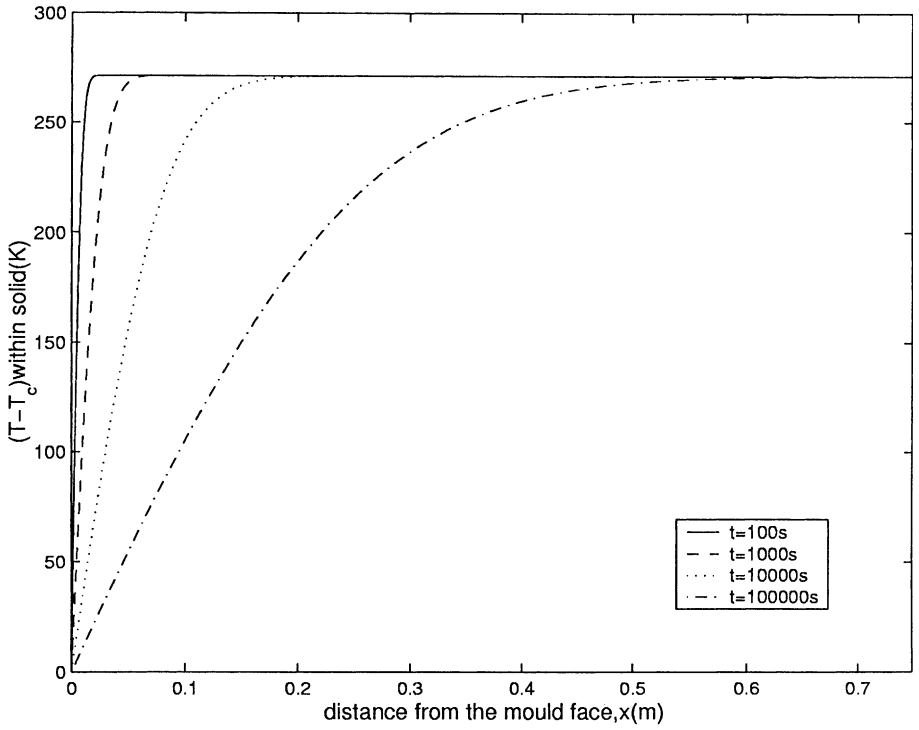

Fig. 6. Temperature distribution within the solid.

$$\frac{\partial^2\theta_S}{\partial x^2} = g^2\frac{d^2\theta_S}{d\eta^2}. \tag{A.2}$$

Substituting Eqs. (A.1) and (A.2) in Eq. (12), one gets

$$\frac{1}{\alpha_S}x\frac{dg}{dt}\frac{d\theta_S}{d\eta} = g^2\frac{d^2\theta_S}{d\eta^2}. \tag{A.3}$$

Substituting $x = \eta/g$ in Eq. (A.3), one obtains

$$\frac{1}{\alpha_S}\eta\frac{d\theta_S}{d\eta} = \frac{g^3}{dg/dt}\frac{d^2\theta_S}{d\eta^2}. \tag{A.4}$$

Since

$$g = \frac{1}{2\sqrt{\alpha_S t}}, \text{ one can write } \frac{g^3}{dg/dt} = -\frac{1}{2\alpha_S}. \tag{A.5}$$

Substituting Eq. (A.5) in Eq. (A.4),

$$\frac{d^2\theta_S}{d\eta^2} + 2\eta\frac{d\theta_S}{d\eta} = 0 \quad \text{for } 0 < \eta < \eta_S. \tag{16}$$

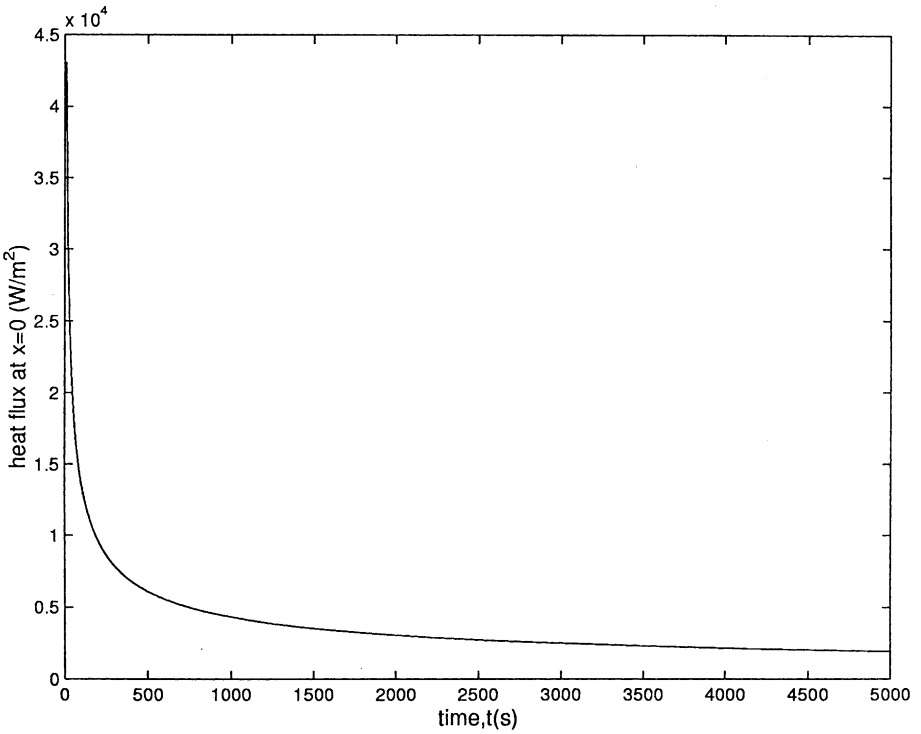

Fig. 7. Variation of boundary heat flux ($x = 0$) with time.

Regarding temperature distribution in the mushy region governed by Eqs. (13) and (14), the partial derivatives are transformed into ordinary derivatives of the similarity variable η as:

$$\frac{\partial \theta_M}{\partial t} = x \frac{dg}{dt} \frac{d\theta_M}{d\eta}, \tag{A.6}$$

$$\frac{\partial^2 \theta_M}{\partial x^2} = g^2 \frac{d^2 \theta_M}{d\eta^2}. \tag{A.7}$$

Substituting Eqs. (A.6) and (A.7) in Eq. (13), one gets

$$\frac{1}{\alpha'_M} x \frac{dg}{dt} \frac{d\theta_M}{d\eta} = g^2 \frac{d^2 \theta_M}{d\eta^2}. \tag{A.8}$$

Substituting $x = \eta/g$ in Eq. (A.8), one obtains

$$\frac{1}{\alpha'_M} \eta \frac{d\theta_M}{d\eta} = \frac{g^3}{dg/dt} \frac{d^2 \theta_S}{d\eta^2}. \tag{A.9}$$

Using Eq. (A.5) in Eq. (A.9), one obtains

$$\frac{d^2 \theta_M}{d\eta^2} + 2 \frac{\alpha_S}{\alpha_{M'}} \eta \frac{d\theta_M}{d\eta} = 0 \quad \text{for } \eta_S < \eta < \eta_L, \tag{17}$$

where α_S/α'_M can be simplified using Eq. (14) and $\alpha = k/(\rho c)$ as

$$\frac{\alpha_S}{\alpha'_M} = \frac{k_S \rho_M c_M}{k_M \rho_S c_S} - \frac{\rho L k_S}{\rho_S c_S k_M} \frac{\partial g_S}{\partial T_M}. \tag{A.10}$$

Now, from the assumption made regarding the constancy of densities, $\rho_S = \rho_L = \rho_M = \rho$ (say), which leads to the following simplified form of Eq. (A.10):

$$\frac{\alpha_S}{\alpha_{M'}} = \frac{c_M - L(\partial g_S/\partial T_M)}{c_S(k_M k_S)}. \tag{18}$$

Regarding temperature distribution in the liquid phase (Eq. (15)), the same similarity transformation as above yields

$$\frac{\partial \theta_L}{\partial t} = x \frac{dg}{dt} \frac{d\theta_L}{d\eta}, \tag{A.11}$$

$$\frac{\partial^2 \theta_L}{\partial x^2} = g^2 \frac{d^2 \theta_L}{d\eta^2}. \tag{A.12}$$

Substituting Eqs. (A.11) and (A.12) in Eq. (15), one gets

$$\frac{1}{\alpha_L} x \frac{dg}{dt} \frac{d\theta_L}{d\eta} = g^2 \frac{d^2 \theta_L}{d\eta^2}. \tag{A.13}$$

Substituting $x = \eta/g$ in Eq. (A.13), one obtains

$$\frac{1}{\alpha_L} \eta \frac{d\theta_L}{d\eta} = \frac{g^3}{dg/dt} \frac{d^2 \theta_L}{d\eta^2}. \tag{A.14}$$

Using Eq. (A.5) in Eq. (A.14), one obtains

$$\frac{d^2 \theta_L}{d\eta^2} + 2 \frac{\alpha_S}{\alpha_L} \eta \frac{d\theta_L}{d\eta} = 0 \quad \text{for } \eta_S < \eta < \eta_L. \tag{19}$$

Since $\rho_S = \rho_L$, α_S/α_L in Eq. (19) can be simplified as

$$\frac{\alpha_S}{\alpha_L} = \frac{k_S c_L}{k_L c_S}. \tag{A.15}$$

References

[1] R.H. Tien, G.E. Geiger, A heat transfer analysis of the solidification of a binary eutectic system, ASME J. Heat Transfer 89 (1967) 230–234.
[2] S.H. Cho, J.E. Sunderland, Heat conduction problems with melting or freezing, ASME J. Heat Transfer 91 (1969) 421–426.
[3] J.C. Muehlbauer et al., Transient heat transfer analysis of alloy solidification, ASME J. Heat Transfer 95 (1973) 324–331.
[4] M.N. Ozisik, J.C. Uzzell Jr., Exact solution freezing in cylindrical symmetry with extended freezing temperature range, ASME J. Heat Transfer 101 (1979) 331–339.

[5] M.G. Worster, Solidification of an alloy from a cooled boundary, J. Fluid Mech. 167 (1986) 481–501.
[6] H.S. Carslaw, J.C. Jaeger, Conduction of Heat in Solids, Clarendon Press, London, 1959.
[7] M.N. Ozisik, Heat Conduction, Wiley, New York, 1980.
[8] J. Crank, Free and Moving Boundary Problems, Oxford University Press, Oxford, 1984.
[9] J.D. Chung et al., An analytical approach to the conduction-dominated solidification of binary mixtures, Int. J. Heat Mass Transfer 42 (1999) 373–377.
[10] M. Lacroix, V.R. Voller, Finite difference solutions of solidification phase change problems: transformed versus fixed grids, Numer. Heat Transfer B 17 (1990) 25–41.
[11] M.C. Flemings, Solidification Processing, McGraw-Hill, New York, 1974.
[12] W.D. Bennon, F.P. Incropera, A continuum model for momentum, heat and species transport in binary solid-liquid phase change systems – II, Application to Solidification in a rectangular cavity, Int. J. Heat Mass Transfer 30 (1987) 2171–2187.
[13] V.R. Voller, A.D. Brent, C. Prakash, The modelling of heat, mass and solute transport in solidification systems, Int. J. Heat Mass Transfer 32 (1989) 1719–1731.
[14] S.V. Patankar, Numerical Heat Transfer and Fluid Flow, Hemisphere, Washington, DC, 1980.
[15] D. Poulikakos, Conduction heat transfer, Prentice-Hall, Englewood Cliff, NJ, 1994.